schematic diagram of the experimental setup used for the transmission experiment.

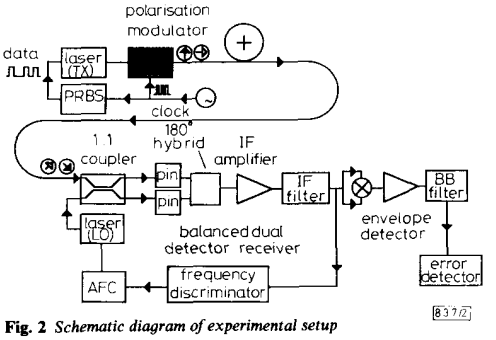

Fig. 2 *Schematic diagram of experimental setup*

Transmission experiments have been carried out with synchronous intrabit polarisation spreading, testing both squarewave and sinusoidal modulating waveforms. The fundamental result was that, as expected from theory, whatever were the polarisation fluctuations introduced by the fibre, the demodulated baseband signal maintained the same level, although the corresponding pulseshape changed. This means that the fraction of transmitted bit signal energy that was heterodyne converted, within each bit interval, was independent of the polarisation transformations along the transmission line, thus demonstrating the feasibility of polarisation insensitive coherent detection by SIB-PS transmission.

The result of BER measurements that have been carried out with S-PS are shown in Fig. 3, showing (in the less favourable polarisation case) a penalty of 4·5 dB (for $BER = 10^{-9}$) with respect to the same system, operated without PS and with manual polarisation control. With respect to the 3 dB loss that

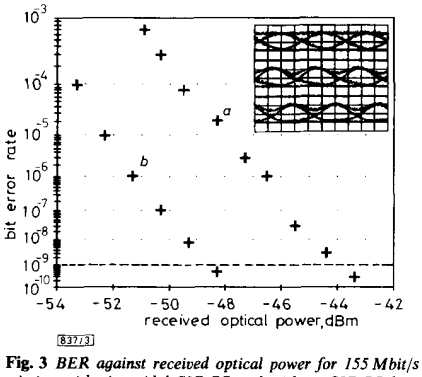

Fig. 3 *BER against received optical power for 155 Mbit/s FSK transmission with sinusoidal SIB-PS and without SIB-PS but with manual polarisation control, for reference*

Different eye diagrams, corresponding to three significant SOP conditions, are shown inset
a With sinusoidal SIB-PS
b Without sinusoidal SIB-PS

is inherent to any polarisation diversity transmission technique, the excess penalty due to the spectrum broadening at intermediate frequency and to nonideal components was kept within 1·5 dB. Similar measurements have been carried out with SQ-PS as well, resulting in an increase of the excess penalty smaller than 1 dB, in agreement with theory.

A noticeable residual effect of SOP fluctuations is the shift of the eye diagram along the time axis, whose extent is bounded within 1/2 bit period, owing to the varying energy distribution inside the bit interval (inset of Fig. 3). As the SOP fluctuations have mechanical or thermal origin, the rate of change is slow and this effect is easily recovered by conventional clock extraction and decision circuits. The second effect resulting from SOP fluctuations is the pulse-shape variation; roughly speaking, the data stream can assume any intermediate configuration between the limit cases of NRZ and RZ waveforms. Proper baseband filtering, resulting in zero-mean output data, allows automatic optimum positioning of the signal with respect to the decision threshold. This is essential to obtain the above mentioned low excess penalties.

Conclusions: The experimental results obtained so far have demonstrated that SIB-PS techniques are feasible and effective, to obtain an FSK coherent link independent of polarisation fluctuations. In particular both the squarewave and the sinusoidal ($\Delta = 137{\cdot}5°$) polarisation spreading approaches have been successfully experimented. A 155 Mbit/s FSK transmission experiment carried out at 1·52 μm has shown an excess penalty within 1·5 dB of the expected performance of the ideal polarisation diversity transmission. This approach can be particularly attractive for the distribution network, due to the inherent simplicity of the corresponding receiver and to the sharing of the polarisation spreading function (exerted inside the transmitter) among a large number of users.

Acknowledgments: This work has been partially supported by the EEC, under Project RACE 1027; within this cooperation, the two-section phase tunable DFB laser diodes have been kindly supplied by D. Leclerc and J. Jacquet of Alcatel Alsthom Research (Marcoussis, France). The authors are also indebted to D. Mazzoni for supplying the decision circuit.

N. CAPONIO
F. DELPIANO
P. GAMBINI
M. PULEO
V. SEANO
E. VEZZONI

CSELT—Centro Studi E Laboratori Telecomunicazioni
Via G. Reiss Romoli, 274, 10148 Torino, Italy

2nd January 1991

References

1 HODGKINSON, T. G., HARMON, R. A., and SMITH, D. W.: 'Polarisation-insensitive heterodyne detection using polarisation scrambling', *Electron. Lett.*, 1987, **23**, (10), pp. 513–514
2 MARONE, G., POGGIOLINI, P., and VEZZONI, E.: 'Polarisation independent detection by synchronous polarization switching in optical coherent systems'. ICC SuperComm 90 (Atlanta, April 1990), Paper 345.3, pp. 1658–1662
3 CALVANI, R., CAPONI, R., MARONE, G., and POGGIOLINI, P.: 'High speed polarisation modulation through an optical guided-wave two-by-two switch'. Proc. of SPIE Conf. on Coherent Lightwave Communications, Boston, 7th–8th September 1989, SPIE Vol. 1175, pp. 89–99
4 JACQUET, J., PAINGT, F., LE GOUEZIGOU, L., LEBLOND, F., LABOURIE, C., LECLERC, D., and PROVEST, J. G.: 'Réponse en modulation de fréquence de laser DFB à deux électrodes'. JNOG90, Grenoble France

EFFECT OF RANDOM ERRORS IN ANTENNA CYLINDRICAL NEAR-FIELD MEASUREMENTS

Indexing terms: Antennas, Measurement, Errors

A closed expression for the autocorrelation of the far field noise due to random near field noise in a cylindrical near to far field transformation is derived. This expression is employed to obtain bounds for the computed radiation pattern for a given near field signal to noise ratio.

Introduction: Near field antenna pattern measurement has become a widely employed technique over the past years. In near field testing the radiation pattern is obtained after processing the antenna near fields scanned over a nearby surface. Common scanning surfaces are planar, cylindrical and spherical. Random noise although quite small will set a fundamen-

tal limit in antenna measurement. This is especially true in low-sidelobe antennas. So far expressions are available[1,2] that relate the near field S/N ratio to the far field S/N ratio for the planar case. Although these expressions provide good estimates, they are not valid in the cylindrical near field. Moreover, the far field S/N ratio, although a quite appealing simple parameter, hides in its simplicity some important aspects.

The far field noise is a stochastic process, and it will be shown that for white Gaussian, space stationary, near field noise, the far field noise is Gaussian and nonstationary in elevation and coloured in azimuth, with a variance dependent on the measurement probe.

Once the far field noise is characterised it is possible to find a 'probability strip', that is an upper and lower bound for the radiation pattern with a given probability. In this way a deeper understanding of the effect of random noise is achieved.

Mathematical development: The theory of cylindrical near field measurements has been well developed elsewhere.[3,4] In this Section, we will employ those expressions necessary to develop the error formulation.

The near to far field transformation is a linear operator, so the effect of an additive noise can be analysed by superposition. The near field noise is assumed to be a complex Gaussian process, space stationary, with zero mean and variance σ^2.

The cylindrical near to far field transformation is based on obtaining the cylindrical modal coefficients of the fields. The first step is the Fourier transform of the near field. If $n(z_i, \phi_j)$ is the measured noise, the discrete Fourier transform (DFT) is

$$N(k_z, n) = \frac{\Delta z\, \Delta\phi}{2\pi} \sum_{i}^{N_z} \sum_{j}^{N_\phi} n(z_i, \phi_j) e^{jk_z z_i} e^{-jn\phi_j} \tag{1}$$

The autocorrelation of the DFT of the noise is[5]

$$\begin{aligned} R_N(p, q) &= \left(\frac{\Delta\phi\, \Delta z}{2\pi}\right)^2 \sigma^2 \sum_{i}^{N_z} \sum_{j}^{N_\phi} e^{-jp\phi_j} e^{jqz_i} \\ &= N_z N_\phi \sigma^2 \left(\frac{\Delta\phi\, \Delta z}{2\pi}\right)^2 \delta(p, q) \end{aligned} \tag{2}$$

that is a white Gaussian noise, because the spectral power density is flat. The cylindrical modal coefficients are found as

$$\begin{aligned} a_n(k_z) &= \frac{N_h b_n^{(2)}(k_z) - N_v b_n^{(1)}(k_z)}{a_n^{(1)}(k_z) b_n^{(2)}(k_z) - a_n^{(2)}(k_z) b_n^{(1)}(k_z)} \\ b_n(k_z) &= \frac{N_v a_n^{(1)}(k_z) - N_h b_n^{(2)}(k_z)}{a_n^{(1)}(k_z) b_n^{(2)}(k_z) - a_n^{(2)}(k_z) b_n^{(1)}(k_z)} \end{aligned} \tag{3}$$

where $a_n^{(i)}(k_z)$ and $b_n^{(i)}(k_z)$ are the modal coefficients of the probe that can be computed as in References 3 or 4, and N_h and N_v are the DFT of the noise in the horizontal and vertical channel.

In this case the coefficients $a_n(k_z)$ and $b_n(k_z)$ are random variables with autocorrelation

$$\begin{aligned} R_{b_n}(p, q) &= \frac{|a_n^{(1)}(k_z)|^2 + |a_n^{(2)}(k_z)|^2}{|a_n^{(1)}(k_z) b_n^{(2)}(k_z) - a_n^{(2)}(k_z) b_n^{(1)}(k_z)|^2} \\ &\quad \times \sigma^2 N_z N_\phi \left(\frac{\Delta\phi\, \Delta z}{2\pi}\right)^2 \delta(p, q) \end{aligned} \tag{4}$$

and

$$\begin{aligned} R_{a_n}(p, q) &= \frac{|b_n^{(2)}(k_z)|^2 + |b_n^{(1)}(k_z)|^2}{|a_n^{(1)}(k_z) b_n^{(2)}(k_z) - a_n^{(2)}(k_z) b_n^{(1)}(k_z)|^2} \\ &\quad \times \sigma^2 N_z N_\phi \left(\frac{\Delta\phi\, \Delta z}{2\pi}\right)^2 \delta(p, q) \end{aligned} \tag{5}$$

Now $a_n(k_z)$ and $b_n(k_z)$ are Gaussian random variables with zero mean, but are not stationary as their autocorrelation is a function of n and k_z. Each far field component is obtained as

$$\begin{aligned} n_\theta(k_z, \phi) &= \sum_{n}^{N_\phi} b_n(k_z) e^{jn\phi} \\ n_\phi(k_z, \phi) &= \sum_{n}^{N_\phi} a_n(k_z) e^{jn\phi} \end{aligned} \tag{6}$$

the autocorrelation of the θ far field noise component is

$$\begin{aligned} R_{n_\theta}(\tau, \xi) &= E\{n_\theta(k_z + \tau, \phi + \xi) n_\theta^*(k_z, \phi)\} \\ &= \sum_m \sum_n R_{b_n}(n - m, \tau) e^{j(n-m)\phi} e^{jn\xi} \end{aligned} \tag{7}$$

as $R_{b_n}(m - n, \tau)$ is zero if $n \neq m$

$$\begin{aligned} R_{n_\theta}(\tau, \xi) &= \sigma^2 N_z N_\phi \left(\frac{\Delta\phi\, \Delta z}{2\pi}\right)^2 \\ &\quad \times \sum_n \frac{|a_n^{(1)}(k_z)|^2 + |a_n^{(2)}(k_z)|^2}{|a_n^{(1)}(k_z) b_n^{(2)}(k_z) - a_n^{(2)}(k_z) b_n^{(1)}(k_z)|^2} e^{jn\xi} \delta(\tau) \end{aligned} \tag{8}$$

The far field noise is white Gaussian and nonstationary in k_z, because the autocorrelation is a function of k_z, and stationary and coloured in ϕ because the autocorrelation is nonzero for $\xi \neq 0$. The far field noise variance for each polarisation is

$$\begin{aligned} \sigma_{ff\theta}^2(k_z, \phi) &= \sigma^2 N_z N_\phi \left(\frac{\Delta\phi\, \Delta z}{2\pi}\right)^2 \\ &\quad \times \sum_n \frac{|a_n^{(1)}(k_z)|^2 + |\alpha_n^{(2)}(k_z)|^2}{|a_n^{(1)}(k_z) b_n^{(2)}(k_z) - a_n^{(2)}(k_z) b_n^{(1)}(k_z)|^2} \\ \sigma_{ff\phi}^2(k_z, \phi) &= \sigma^2 N_z N_\phi \left(\frac{\Delta\phi\, \Delta z}{2\pi}\right)^2 \\ &\quad \times \sum_n \frac{|b_n^{(1)}(k_z)|^2 + |b_n^{(2)}(k_z)|^2}{|a_n^{(1)}(k_z) b_n^{(2)}(k_z) - a_n^{(2)}(k_z) b_n^{(1)}(k_z)|^2} \end{aligned} \tag{9}$$

From the expressions above, the effect of an additive Gaussian white noise in the near field is an additive Gaussian noise with variance proportional to the near field noise variance and function of k_z. Moreover the variance depends on the probe cylindrical coefficients (radiation pattern), so the effects of the noise will be dependent on the probe and in general different for each polarisation. It is important to notice that the expressions (eqn. 9) can be easily evaluated in the transformation process because the probe cylindrical coefficients are also required to perform the probe correction.

Expected value of radiation pattern: The noise contaminated radiation pattern will be of the form

$$\tilde{E}(k_z, \phi) = \tilde{E}(k_Z, \phi) + \tilde{n}(k_z, \phi) \tag{10}$$

where $\tilde{n}(k_z, \phi)$ is a Gaussian noise with variance $\sigma_{ff}^2(k_z)$ given by eqn. 9. The far field module is for a given polarisation

$$\begin{aligned} |\tilde{E}| &= |\mathscr{R}(E + n) + j\mathscr{I}(E + n)| \\ &= (\mathscr{R}(E + n)^2 + \mathscr{I}(E + n)^2)^{1/2} \\ &= (X^2 + Y^2)^{1/2} \end{aligned} \tag{11}$$

where X and Y are the real and imaginary parts of $E(k_z, \phi) + n(k_z, \phi)$. X and Y are Gaussian random variables with mean value $\mathscr{R}(E)$ and $\mathscr{I}(E)$, and variance σ_{re}^2 and σ_{im}^2, respectively, and

$$\sigma_{re}^2 = \sigma_{im}^2 = \tfrac{1}{2}\sigma_{ff}^2 \tag{12}$$

$|\tilde{E}|$ is a random variable with a Rice probability density function (PDF) given by[6]

$$f(|\tilde{E}|) = \frac{|\tilde{E}|}{\sigma_{re}^2} e^{-(|E|^2 + |E|^2)/2\sigma_{re}^2)} I_0\left(\frac{|\tilde{E}|\,|E|}{\sigma_{re}^2}\right) \tag{13}$$

where I_0 is the modified Bessel function of order zero. When $(|E|^2/\sigma_{re}^2) \gg 1$ the Rice PDF can be approximated by a Gaussian PDF with mean value $|E|$, on the other hand if $(|E|^2/\sigma_{re}^2) \ll 1$ we have a Rayleigh PDF with mean value $\sigma_{re}\sqrt{(\pi/2)}$. Notice that in the latter case the value of the obtained far field pattern is independent of the real value of the radiation pattern.

Knowing the PDF of the module of the far field, an upper and lower bound M and m for $|\tilde{E}|$ can be calculated by

$$P(|\tilde{E}| \leq M) = \int_0^M f(|\tilde{E}|)\, d|\tilde{E}| = p \tag{14}$$

$$P(|\tilde{E}| > m) = 1 - \int_0^m f(|\tilde{E}|)\, d|\tilde{E}| = q \tag{15}$$

where p and q are the probabilities of not exceeding the bound M and of exceeding m, respectively. The probability that the far field is between M and m is

$$P(m < |\tilde{E}| \leq M) = \int_m^M f(|\tilde{E}|)\, d|\tilde{E}| = p + q - 1 \tag{16}$$

Results: Fig. 1 shows a low sidelobe radiation pattern, and the upper and lower bound for a 90% probability when the near field S/N ratio is 40 dB. An error smaller than 8 dB is predicted in the first sidelobe, and the other sidelobes will be practically smeared by the noise. Fig. 2 shows the resultant radiation pattern for the same antenna when the near field S/N ratio is effectively 40 dB. The radiation pattern is bounded by the computed limits.

Conclusions: A new expression has been found that relates the statistical characteristics of a far field noise to the near field noise. It has been shown that the far field noise is dependent on the measurement probe. Once the noise is characterised, it is possible to obtain meaningful bounds for the radiation pattern, that allow the prediction of the effect of random errors in the computed far field.

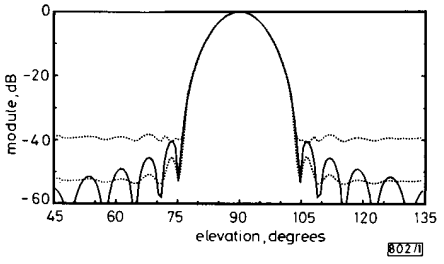

Fig. 1 *Copolar radiation pattern for low sidelobe antenna and 90% bounds for 40 dB near field S/N ratio*

——— low sidelobe radiation pattern
····· upper and lower bounds for 90% probability when near field S/N ratio = 40 dB

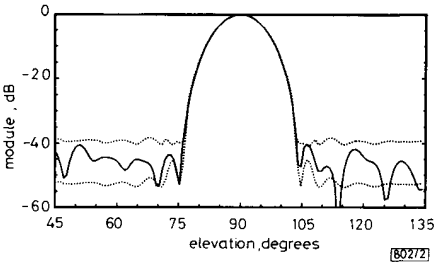

Fig. 2 *Computed copolar radiation pattern when near field S/N ratio is 40 dB*

——— radiation pattern
····· computational limits

J. ROMEU
L. JOFRE

Department of Signal Theory and Communications
Universitat Politecnica de Catalunya
Aptat. 32002. 08080 Barcelona, Spain

17th December 1990

References

1 NEWEL, A. C., and STUBENRAUCH, C. F.: 'Effect of random errors in planar near-field measurement', *IEEE Trans.*, June 1988, **AP-36**, pp. 769–773
2 HOFFMAN, J. B., and GRIMM, K. R.: 'Far-field uncertainty due to random near-field measurement error', *IEEE Trans.*, June 1988, **AP-36**, pp. 774–780
3 PAPOULIS, A.: 'Probability, random variables, and stochastic processes' (McGraw-Hill, New York, 1965)
4 LEACH, W. M., and PARIS, D. T.: 'Probe compensated near-field measurements on a cylinder', *IEEE Trans.*, July 1973, **AP-21**, pp. 435–446
5 BORGIOTTI, G. V.: 'Integral equation formulation for probe corrected far-field reconstruction from measurements on a cylinder', *IEEE Trans.*, July 1978, **AP-26**, pp. 572–578
6 NORTH, D. O.: 'An analysis of the factors which determine signal/noise discrimination in pulsed-carrier systems', *Proc. IEEE*, July 1963, **51**, pp. 1016–1027

LOGARITHMIC GAIN/CURRENT-DENSITY CHARACTERISTIC OF InGaAs/InGaAlAs/InP MULTI-QUANTUM-WELL SEPARATE-CONFINEMENT-HETEROSTRUCTURE LASERS

Indexing terms: Semiconductor lasers, Lasers

The threshold current density of InGaAs/InGaAlAs/InP SCH MQW lasers with various cavity lengths and numbers of wells has been measured. The gain of each well depends logarithmically on current density from 200 to at least 2000 A cm^{-2}. Curves are presented for optimising the number of wells. Comparisons are made with GaAs/AlGaAs MQW lasers.

Introduction: McIlroy, Kurobe and Uematsu[1] analysed the theoretical gain characteristics for multi-quantum-well (MQW) lasers. They showed that when the well width is narrow enough to neglect the population of the higher energy levels, the relationship between gain G and current density J can be reduced to the simple form

$$G = G_0[1 + \ln(J/J_0)] \tag{1}$$

G_0 and J_0 are constants which correspond to the point on this characteristic where G/J is greatest. A knowledge of G_0 and J_0 and the gain requirement of the cavity is sufficient to derive the optimum number of wells for any GaAs/AlGaAs MQW laser. However one cannot assume, *a priori*, that this method is applicable to lasers with InGaAs quantum wells. The current density J in eqn. 1 is associated with radiative processes. In InGaAs lasers the threshold current includes a considerable additional contribution associated with nonradiative effects such as Auger recombination, in a proportion that increases as the threshold rises. Hence eqn. 1 should have a more complicated and less general form when expressed in terms of total current density, and the simple optimisation procedure might no longer apply.

Device structure: It has been recently demonstrated[2,3] that InGaAlAs barrier layers in conjunction with InGaAs quantum wells can provide threshold current densities in